PCCP

Accepted Manuscript

ROYAL SOCIETY OF CHEMISTRY

www.rsc.org/pccp

Journal Name

ARTICLE TYPE

Cite this: DOI: 10.1039/xxxxxxxxxx

Strain and temperature dependent absorption spectra studies in identifying phase structure and band gap of $EuTiO_3$ perovskite films†

Kai Jiang,[a,b] Run Zhao,[c] Peng Zhang,[a] Qinglin Deng,[a] Jinzhong Zhang,[a] Wenwu Li,[a] Zhigao Hu,*[a] Hao Yang,[d] and Junhao Chu [a]

Received Date
Accepted Date

DOI: 10.1039/xxxxxxxxxx

www.rsc.org/journalname

Post-annealing has been approved to effectively relax the out-of-plane strain in thin films. Epitaxial $EuTiO_3$ (ETO) thin films, with and without strain, have been fabricated on (001) $LaAlO_3$ substrates by pulsed laser deposition. The absorption and electronic transitions of the ETO thin films are investigated by means of temperature dependent transmittance spectra. The antiferrodistortive phase transition can be found at about 260∼280 K. The first-principles calculations indicate there are two interband electronic transitions in ETO films. Remarkably, the direct optical band gap and higher interband transition for ETO films have variation trends with different strain and temperature. The strain leads to a band gap shrink of about 240 meV while the higher interband transition expansion of about 140 meV. The hardening of the interband transition energies in ETO films with increasing temperature can be attributed to the Fröhlich electron-phonon interaction. The behavior can be linked to the strain and low temperature modified the valence electronic structure, which is associated with rotations of the TiO_6 octahedra.

1 Introduction

Multiferroic materials have cultivated a great deal of interest in recent years due to their complex magneto-dielectric and multiferroic properties arising from multiple coupled order parameters existing in a single system.[1,2] Among these materials, europium titanate perovskite $EuTiO_3$ (ETO) is considered as the strongest novel multiferroic material known today.[3–5] One interesting finding is that bulk ETO (single crystal or ceramic) is not multiferroic. It is a quantum paraelectric with *G*-type antiferromagnetic order below the Néel temperature T_N∼5.3 K.[6–10] The state originates from superexchange interactions between Eu 4*f* spin via Ti 3*d* orbitals. However, epitaxial ETO films may become both ferroelectric (FE) and ferromagnetic (FM) for large enough misfit strain.[3,4] The FM state is induced by supplying conduction electrons to the otherwise empty Ti 3*d* orbitals. It is known that bulk ferroic oxides are brittle and will crack under moderate strains, typically 0.1%, while strain of about ±3% are common in epitaxial oxide films. Moreover, it has also proven that the epitaxial ETO films with different compressive/tensile strains, deposited on $DyScO_3$ (DSC) or $(LaAlO_3)_{0.3}$-$(SrAl_{0.5}Ta_{0.5}O_3)_{0.7}$ (LSAT), present several novel equilibrium phases.[4,11,12] On the other hand, epitaxial strain has been used to greatly enhance the mobility of transistors, increase catalytic activity, and significantly increase superconducting, ferromagnetic, and ferroelectric transition temperatures.[13–18] Therefore, it is interesting for us to to conduct a more thorough investigation on the physical behavior of high-quality ETO thin films.

Considering the preparation process of thin films, extrinsic effects have important influence on their physical properties.[3,11–13] Recently, Lee *et al.* actually confirmed the theoretical prediction and revealed ferroelectric and ferromagnetic order in the tensile-strained ETO thin films.[3] A strong in-plane uniaxial magnetic anisotropy in a strain-enabled multiferroic $EuTiO_3$ thin film epitaxially grown on a (110) DSC substrate was observed by Xe *et al.*.[12] Zhao *et al.* demonstrated that the post-annealing for ETO thin films effectively decreases the leakage current by reducing Eu^{3+} impurities.[16] However, previous experimental and theoretical studies on ETO films have focused on their ferroelectric or ferromagnetic behaviors,[3,8,13,16] while neglected the optical properties. If optical properties in ETO could be controlled, it would be useful for future applications, such as nonvolatile ferroelectric memories and many other advanced photonic devices. Therefore, the strain and temperature effects on the optical response

[a] *Key Laboratory of Polar Materials and Devices, Ministry of Education, Department of Electronic Engineering. East China Normal University, Shanghai 200241, China.*
[b] *National Laboratory for Infrared Physics, Shanghai Institute of Technical Physics, Chinese Academy of Science, Shanghai 200083, China.*
[c] *School of Mathematics and Physics and Research Center for Solid State Physics and Materials, Suzhou University of Science and Technology, Suzhou 215009, China.*
[d] *College of Science, Nanjing University of Aeronautics and Astronautics, Nanjing 211106, China.*
Tel: +86-21-54345150; Fax: +86-21-54345119; E-mail: zghu@ee.ecnu.edu.cn

behavior and electronic band structure need to be systematically investigated. Fortunately, optical spectroscopy is a sensitive and microscopic probe of the nature and size of a band gap, chemical bonding, and hybridization.[19–21] It is possible to clarify the optical properties and electronic band structures for high quality epitaxial ETO films.

In this paper, we present a detailed investigation of the structure, surface morphology, optical absorption and band structure in strained (*s*-ETO) and unstrained (*u*-ETO) ETO films. The optical measurements demonstrate that the out-of-plane strain can control the antiferrodistortive phase transition temperature and induce a modification of the valence electric structures for epitaxial ETO films.

2 Experimental details

The ETO films were grown on (001)-oriented $LaAlO_3$ (LAO) substrates using pulsed laser deposition (PLD). A high-density ETO ceramic target, synthesized by solid-state reaction using mechanochemical activation before calcination, was focused by a plused excimer laser (Lambda Physik, 248 nm, 3 Hz, 2 J/cm^2). The deposition temperature was kept at 650 °C and oxygen pressure was 1×10^{-4} Pa. It should be pointed out that part of films were post-annealed at 1000 °C under a flowing gas of 95 vol. %Ar+5 vol. %H_2 for 8.5 h in order to relax the out-of-plane lattice strain after deposition. Details about the film growth, microstructure and characterization can be found elsewhere.[16]

The crystalline structure and surface morphology of ETO thin films were determined by the high resolution X-ray diffraction (XRD, Rigaku D/MAX 2000PC), scanning electron microscope (SEM, Philips S-3000N XL30FEG) and atomic force microscope (AFM, Bruker Dimension Icon). The temperature dependent transmittance spectra were recorded on heating by a double beam near infrared-ultraviolet spectrometer (PerkinElmer UV/VIS Lambda 950) in the photon energy range of 190-2650 nm (0.5-6.5 eV) with an interval of 2 nm. The films were mounted into an optical cryostat (Janis SHI-4-1) for the low temperature measurements from 10 to 300 K with a step of 10 K.

3 Results and discussion

Figs. 1(a) and (b) illustrates the XRD pattern of the as-deposited and annealed ETO thin films deposited on (001) LAO substrates at room temperature. For both of the ETO films, the (00*l*) reflections are observed together with the (00*l*) LAO substrate reflections. In other words, the epitaxial ETO phase has been grown along the (001) orientation. It should be pointed out that the lattice constant of ETO single crystal (3.905 Å) is larger than that of LAO (3.790 Å). The (00*l*) peaks from the annealed ETO films shift toward a higher angle side, which is similar with the ETO films deposited on $SrTiO_3$ (STO) substrates.[15,22] These results indicate that out-of-plane lattice constant of the annealed ETO film shrinks (from 3.984 Å to 3.902 Å according to the Debye-Scherrer method, nearly as the same as bulk ETO material) along the *c*-axis determined by the blueshift of the ETO peaks. The increment of the lattice constant is related to the out-of-plane strain during the deposition in high-vacuum, which can be relaxed by the post-annealed process.[16,22] A cross-sectional SEM image of epitaxial

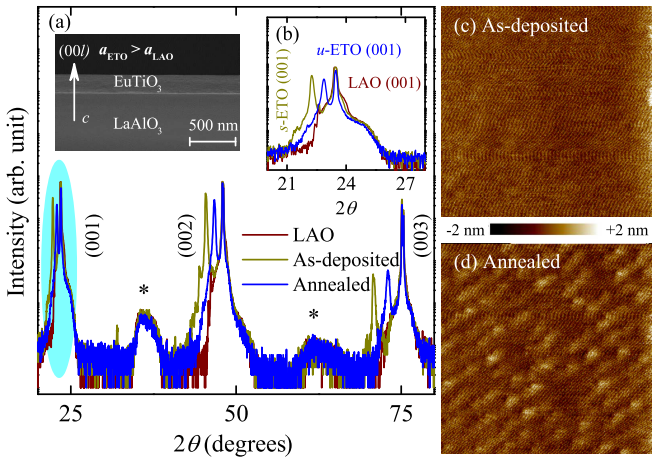

Fig. 1 (a) The XRD patterns of ETO thin films measured at room temperature and it was plotted as the log scale in intensity. The insert shows optical cross sectional micrographs of epitaxial ETO films. The symbol (∗) indicates the observed trace from the LAO substrate. (b) A magnified view near (001) diffraction peaks between the as-deposited (strained) and annealed (unstrained) films. (c) As-deposited and (d) annealed AFM images (1×1 μm^2) of the ETO films grown on LAO (001) substrates.

ETO films is shown in Fig. 1(a). There is a distinct interface between the ETO film and LAO substrate. The thickness of the film is calculated to be ∼217 nm. It has been verified that the lattice misfit strain between the film and substrate decreases in magnitude immediately with increasing the thin film thickness.[23] For the epitaxial ETO film, there is only out-of-plane lattice strain in as-deposited film, instead of the lattice misfit strain. Figs. 1(c) and (d) show the surface morphologies from the two kinds of ETO films. The as-deposited film with strain exhibited the characteristic of two-dimensional growth, reflecting the atomically flat surface of substrates. A stepped and terraced structure is clearly seen in the annealed film without strain. The root-mean-square surface roughness is estimated to 0.462 and 0.391 nm for *s*-ETO and *u*-ETO, respectively, which is corresponding to the size of one unit cell of bulk ETO material. The XRD, SEM and AFM results reveal that the ETO films are commensurate, smooth and of high structural perfection.

Fig. 2(a) shows the absorption coefficient α vs. photon energy for *s*-ETO and *u*-ETO thin films at different temperatures. Note that the absorption spectra are quite different, indicating that the influence of strain in ETO thin film on the optical absorption is significant. The absorption for both of the ETO films exhibits two steep increasing points, consistent with the occurrence of possible interband transitions E_1 and E_2. The temperature effect on the absorption coefficient values for *s*-ETO and *u*-ETO films at 1.8 and 2.8 eV between the two transition energies are plotted in Fig. 2(b) and (c). Note that there are two critical ranges with increasing temperature from 10 to 300 K from the absorption coefficient values. (i) 110∼130 K: a clear break in slope of absorption coefficient, which is consistent with the result by Spalek *et al.* from resonant ultrasound spectroscopy measurements.[11] The mechanism for this might be related to some spin-lattice couplings between strain and local fluctuations of dipoles associated to the incipient

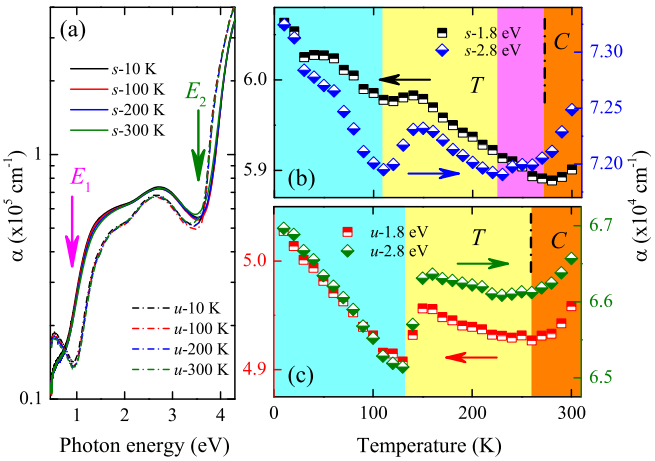

Fig. 2 (a) Temperature dependent optical absorption coefficient α vs. photon energy for s-ETO and u-ETO thin films. The arrows indicate the occurrence of interband electronic transitions. (b) and (c) show absorption coefficient value located at 1.8 eV and 2.8 eV at different temperatures for s-ETO and u-ETO films, respectively.

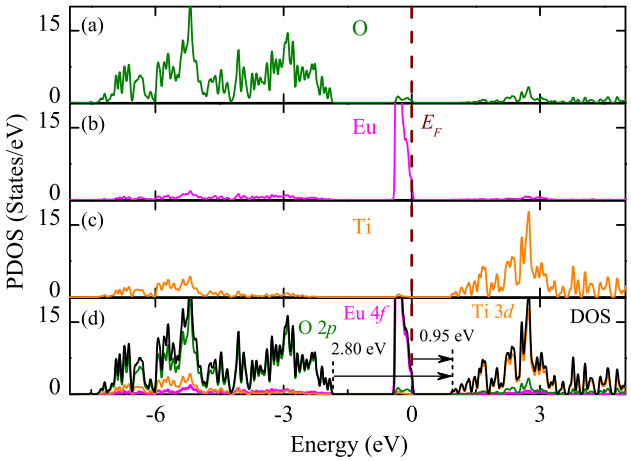

Fig. 3 Magnified view of the up-spin component for the partial density of states (PDOS) of O (a), Eu (b) and Ti (c) atoms of $EuTiO_3$ with the G-type magnetic configuration. (d) Total DOS for ETO in the energy region near the valence band derived from the DFT band structure calculations.

ferroelectric phase transition. (ii) 260∼280 K: a structural antiferrodistortive phase transition, from tetragonal (T) $I4/mcm$ to cubic (C) $Pm\bar{3}m$, involving antiphase tilting of oxygen octahedra along the c axis, in analogy to the case of STO at ∼106 K. It should be pointed out that the critical temperature for the unstrained ETO film is ∼260 K, which is slightly lower than that of strained ETO film (at about 280 K). The absorption data show that the out-of-plane strain enhances the phase transition temperature by ∼20 K owing to the enhanced superexchange interaction.[24] In addition, there may be a disorder-order transition at about 230 K for strained ETO film [see Fig. 2(b)], associated with a divergence of the correlation length of the tetragonal distortion.[25] It indicates that the variation of absorption coefficients is very sensitive to the strain and temperature, which can be useful for characterization of the ETO perovskite structure. The structural and absorption investigations confirmed the antiferrodistortive phase transition in epitaxial ETO films.

In order to investigate the origin of the exchange interaction in ETO electronic structure, the first principles density-functional theory (DFT) calculation based on the generalized gradient approximation (GGA)+U (U is the on-site Coulomb interaction in the Hubbard model) was carried out for ETO with a $\sqrt{2}\times\sqrt{2}\times2$ tetragonal supercell containing 20 atoms. The Peedew-Bruke-Ernzerhof (PBE) functionals are used to address exchange-correlation interactions along with a standard plane-wave basis set. All the calculations are performed with a 430 eV cutoff energy, and $3\times3\times2$ k-point Monkhorst-Pack mesh. The convergence criterion for the electronic energy is 10^{-6} eV. Fig. 3 illustrate the site-projected partial density of states (PDOS) of ETO with the G-type magnetic configuration. The main component of the PDOS in the energy region from -8 to -3 eV is the O $2p$ states, from -0.5 to 0 eV is the Eu $4f$ states, and from 1 to 5 eV is the Ti $3d$ states, as seen in Fig. 3(a)-(c), respectively. The valence band mainly consists of O $2p$ states, while the conduction band chiefly has Ti $3d$ and Eu $5d$ characters. More importantly, the occupied Eu $4f$ bands lying between these bands are narrow, indicating their localized nature. According to the previous literature, most of the $ATiO_3$ perovskites with A=Ca^{2+}, Sr^{2+}, Ba^{2+} and Pb^{2+}, show little contribution of the A-site cations to the low-energy part of the valence band. However, the top of the valence band of the ETO perovskite is comprised of the narrow-band formed by the Eu $4f$ electrons according to the first-principle calculations and recent experiment studies.[14,15,26] From the band structure and density of states (DOS) in Fig. 3(d), two solid arrows indicate the direct electron transitions: Eu $4f$ to Ti $3d$ states located at 0.95 eV and O $2p$ to Ti $3d$ states calculated at 2.80 eV, respectively. The results are in good agreement with those estimated from our optical absorption spectra as following.

The optical band gap and higher interband transition for ETO films, as determined from the absorption coefficient using the Tauc's law, are plotted in Figs. 4(a) and (b), respectively. The band gap in $EuTiO_3$ is expected to form between the occupied Eu $4f$ and empty Ti $3d$ states [see the inset schematic diagram of Fig. 4(a)]. The optical band gap E_1 value in as-deposited and annealed ETO films at 10 K is calculated to be ∼1.05 and 1.29 eV, respectively. The results indicate that the strain leads to a band gap shrink of about 240 meV at low temperature. The higher interband transitions E_2 attributed to the transition from O $2p$ to Ti $3d$ states, are found at about 3.97 and 3.83 eV at 10 K. The obtained interband electronic transitions are in good agreement with the theoretical calculations and previous literatures,[7,14,15] considering that the calculated electronic transitions are underestimated by about 20%-30% based on DFT calculations. It is true that the structure distortion of the film, which could provide the perturbation on the electronic band structure, induce the optical response discrepancy. For the two as-deposited and annealed ETO thin films, the strain induces the higher interband transition expansion of about 140 meV. The different gap results demonstrate that strain plays a key role on modulating the electronic band structures in ETO films, which is compatible with previous

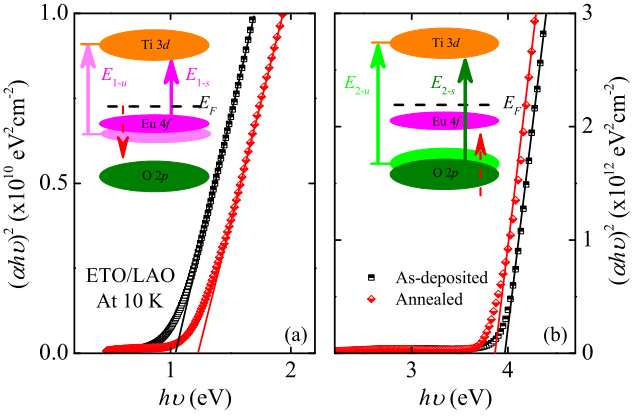

Fig. 4 Plot of $(\alpha h\upsilon)^2$ vs. the photon energy for the interband transitions of the ETO films at 10 K. (a) The direct optical band gap E_1 and (b) a high interband transition energy E_2 were obtained according to the linear extrapolation of $(\alpha h\upsilon)^2$=0. The insets show schematic diagrams of the photo induced interband transitions. Note that the solid and dash arrows indicate the interband transitions and change of the valence electric structures after annealing, respectively.

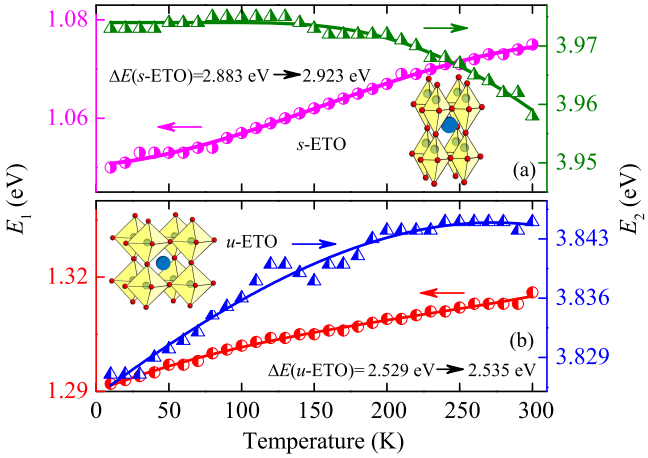

Fig. 5 Temperature dependence of the interband transition energies in the temperature range from 10 K to 300 K for (a) strained and (b) unstrianed ETO thin films, respectively. The solid line for E_2 in s-ETO film corresponds to the fitting from Bose-Einstein model. The hardening of the interband transition energies with temperature is nonlinearly fitted with the solid lines to guide the eyes.

static infrared spectroscopy and femtosecond transient absorption spectroscopy.[15,24]. This phenomena can be attributed to the impurity phase of Eu^{3+} and oxygen vacancies in strained ETO films, leading to an offset for the central ions Ti^{4+} in oxygen octahedron [see the inset schematic diagram of Fig. 5(a)]. The local breaking of symmetry in strained ETO film can introduce a mixing of the oxygen and titanium related bands that leads to a modification of the valence and conduction bands which can directly affect the interband transitions. Moreover, the strength of superexchange interactions between the Eu 4f spins via the Ti 3d states are expected to depend on the octahedral rotations.[1,27] The Ti 3d states are strongly affected by the rotations of the TiO_6 octahedra. The result is that the strain significantly changes the octahedral rotations, which not only reduces the band gaps between the Eu 4f and Ti 3d bands but also raises the higher energy transitions from O 2p to Ti 3d states.

Figs. 5(a) and (b) show the temperature dependent interband transition energies for s-ETO and u-ETO films, respectively, as determined from the optical absorption coefficient. For the strained ETO film, the E_1 value increases and E_2 value decreases as a function of temperature. However, it is found that all of the interband transition energies for the unstrained ETO film increase with the temperature. The phenomena can be ascribed to the electronic band structure variations of the film under the lower temperatures. The E_1 interband transitions have blue shifts from 1.050 to 1.075 eV and 1.292 to 1.316 eV for strained and unstrained ETO films, respectively, indicating a band gap shrink about 25 meV for all the films at low temperature. It should be noted that the interband transitions E_2, associated with the O 2p to Ti 3d transition, show a variation tendency as a function of temperature, which is in good agreement with the optical band gap of STO thin films on DSC or LSAT substrates.[28] Note that there is an obviously anomalous behavior at about 130 K especially for higher interband transition, which is consistent with the results from absorption coefficients, corresponding to the incipient ferroelectric phase transition. The changes of electronic transitions with temperature can be attributed to the thermal expansion of the lattice and electron-phonon interaction, which is caused by the deformation of the electronic potentials due to the dynamic atomic displacements. Note that the thermal expansion effect of the lattices plays a negligible role in the temperature-induced variation in band structure in ferroelectric materials. In particular, the electron-phonon interaction, which includes the contributions from both acoustic as well as optical phonons, is usually the dominating one.[20] Lattice vibration, leading to a deviation of atoms or ions from balance sites, would destroy the lattice periodic field, give rise to additional potential as a perturbation of electron energy and transition, even change the chemical bond length, and then further renormalize band structure and band gap energy.[29] When the temperature increasing, the enhancing lattice vibration, resulting in the more activated population of phonon modes, reinforces the electron-phonon interaction, leading to the different electronic band structure. The temperature dependence of E_2 interband transitions in strained film can be described by the Bose-Einstein model[29,30]:

$$E(T) = E(0) - \frac{2a_B}{exp(\Theta_B/T) - 1}. \quad (1)$$

where $E(0)$ is the transition energy at 0 K, a_B is the strength of the electronÍCphonon interaction and $\Theta_B = \hbar\nu/k_B$ is the characteristic temperature representing the effective phonon energy on the temperature scale. The $E_2(T = 0K)$ is estimated to be about 3.974 eV. The parameters a_B and Θ_B in eq (1) are 216 meV and 1018 K, respectively. It is found that the parameters are larger than that from the multiferroic material $BiFeO_3$ (21 meV and 238 K), suggesting that the longitudinal optical phonon replicas of the exciton transition are expected to be enhanced in ETO films. The observed hardening of the interband transition energies with temperature can be attributed to the Fröhlich electron-phonon interaction, which is consistent with the similar quantum-paraelectric

bulk materials such as STO, $CaTiO_3$, and $KTaO_3$.[28] The Fröhlich interaction arises from the long wavelength longitudinal optical phonons which give rise to a macroscopic polarization. It can describe the shift of the transition energies[28]:

$$\Delta E = -m(\varepsilon_\infty^{-1} - \varepsilon_0^{-1})(1 + \frac{2}{exp(\Theta_B/T) - 1}). \quad (2)$$

where ε_∞ and ε_0 are the dielectric constants at energies well above and below the phonon range, respectively, and m is a temperature independent prefactor that depends on material parameters such as effective mass and lattice constant. Thus, the mechanism of the Fröhlich interaction in ETO films needs to replenish by tempearture dependent spectroscopic ellipsometry studies in the future. Moreover, the hardening phenomenon can also be attributed to the existence of localized $4f$ moments on the Eu^{2+} site in ETO perovskite material. Unlike other $ATiO_3$ perovskite ferroelectric materials, the superexchange interaction between the Eu $4f$ spins via Ti $3d$ bands in ETO films, associated to the rotations of the TiO_6 octahedra, could be affected by the temperature. Therefore, it may change the interband transitions from the valence band of Eu $4f$ and O $2p$ orbitals. On the other hand, the difference value between the optical band gap and higher interband transition ΔE(s-ETO) increases from 2.883 to 2.923 eV with decreasing temperature, suggesting a valence electronic structure expansion of 40 meV between Eu $4f$ and O $2p$ bands under the low temperature. The difference value in unstrained ETO films is about 2.530 eV, which shows no significant changes with the temperature. Accordingly, the out-of-plane strain, not only controls the antiferrodistortive phase transition temperature but also leads to blue/red shifts of the interband electronic transitions from valence Eu $4f$ and O $2p$ bands to conduction Ti $3d$ bands, in conjunction with the low temperature effects.

4 Conclusions

To summarize, the strained and unstrained ETO thin films on (001)-oriented LAO substrates were fabricated by pulsed laser deposition. From temperature dependence of absorption spectra, it was found that some hints of an antiferrodistortive phase transition from tetragonal to cubic were clearly observed. The two electronic transitions obtained by the first principles calculations are in good agreement with that estimated from our optical absorption spectra. The strain in epitaxial ETO films, suggesting a structural distortions associated with rotations of TiO_6 octahedra, plays an important role in modification of the electronic band structures. The variation temperature dependent interband transitions can be attributed to the Fröhlich electron-phonon interaction. Thus, the absorption spectroscopy is a very promising tool for a study of the electronic band structures as well as of structural phase transitions in thin films.

Acknowledgment

One of the authors (K. Jiang) is grateful to Kai Shi, Kai Tang and Junyong Wang for the technical supports. This work was financially supported by Major State Basic Research Development Program of China (Grant Nos. 2011CB922200, 2013CB922300 and 2014CB921002), the Natural Science Foundation of China (Grant Nos. 11374097, 61376129, 11274237, and 11374225), Projects of Science and Technology Commission of Shanghai Municipality (Grant Nos. 15JC1401600, 14XD1401500, 13JC1402100, and 13JC1404200), the Program for Professor of Special Appointment (Eastern Scholar) at Shanghai Institutions of Higher Learning, and the Priority Academic Program Development of Jiangsu Higher Education Institutions and the USTS Cooperative Innovation Center for Functional Oxide Films and Optical Information.

References

1 H. Akamatsu, Y. Kumagai, F. Oba, K. Fujita, H. Murakami, K. Tanaka, and I. Tanaka, *Phys. Rev. B*, 2011, **83**, 214421.
2 R. Ramesh and N. A. Spaldin, *Nat. Mater.*, 2007, **6**, 21-29.
3 J. H. Lee, L. Fang, E. Vlahos, X. Ke, Y. W. Jung, L. F. Kourkoutis, J.-W. Kim, P. J. Ryan, T. Heeg, M. Roeckerath, V. Goian, M. Bernhagen, R. Uecker, P. C. Hammel, K. M. Rabe, S. Kamba, J. Schubert, J. W. Freeland, D. A. Muller, C. J. Fennie, P. Schiffer, V. Gopalan, E. Johnston-Halperin, and D. G. Schlom, *Nature*, 2010, **466**, 954-958.
4 Y. Yang, W. Ren, D. Wang, and L. Bellaiche, *Phys. Rev. Lett.*, 2012, **109**, 267602.
5 K. Shimamoto, K. Hatabayashi, Y. Hirose, S. Nakao, T. Fukumura, and T. Hasegawa, *Appl. Phys. Lett.*, 2013, **102**, 042902.
6 H. Akamatsu, K. Fujita, H. Hayashi, T. Kawamoto, Y. Kumagai, Y. Zong, K. Iwata, F. Oba, I. Tanaka, and K. Tanaka, *Inorg. Chem.*, 2012, **51**, 4560-4567.
7 J. H. Lee, X. Ke, N. J. Podraza, L. F. Kourkoutis, T. Heeg, M. Roeckerath, J. W. Freeland, C. J. Fennie, J. Schubert, D. A. Muller, P. Schiffer, and D. G. Schlom, *Appl. Phys. Lett.*, 2009, **94**, 212509.
8 H. Akamatsu, Y. Kumagai, F. Oba, K. Fujita, K. Tanaka, and I. Tanaka, *Adv. Funct. Mater.*, 2013, **23**, 1864-1872.
9 V. Goian, S. Kamba, O. Pacherová, J. Drahokoupil, L. Palatinus, M. Dušek, J. Rohlíček, M. Savinov, F. Laufek, W. Schranz, A. Fuith, M. Kachlík, K. Maca, A. Shkabko, L. Sagarna, A. Weidenkaff, and A. A. Belik, *Phys. Rev. B*, 2012, **86**, 054112.
10 T. Birol and C. J. Fennie, *Phys. Rev. B*, 2013, **88**, 094103.
11 L. J. Spalek, S. S. Saxena, C. Panagopoulos, T. Katsufuji, J. A. Schiemer, and M. A. Carpenter, *Phys. Rev. B*, 2014, **90**, 054119.
12 X. Ke, T. Birol, R. Misra, J. H. Lee, B. J. Kirby, D. G. Schlom, C. J. Fennie, and J. W. Freeland, *Phys. Rev. B*, 2013, **88**, 094434.
13 D. G. Schlom, L.-Q. Chen, C. J. Fennie, V. Gopalan, D. A. Muller, X. Pan, R. Ramesh, and R. Uecker, *MRS Bull.*, 2014, **39**, 118-130.
14 T. Kolodiazhnyi, M. Valant, J. R. Williams, M. Bugnet, G. A. Botton, N. Ohashi, and Y. Sakka, *J. Appl. Phys.*, 2012, **112**, 083719.
15 Z. G. Li, R. Zhao, W. Li, H. Wang, H. Yang, and Y. L. Song, *Appl. Phys. Lett.*, 2014, **105**, 162904.
16 R. Zhao, W. W. Li, L. Chen, Q. Q. Meng, J. Yang, H. Wang, Y. Q. Wang, R. J. Tang, and H. Yang, *Appl. Phys. Lett.*, 2012, **101**, 102901.

17 T. Yamamoto, R. Yoshii, G. Bouilly, Y. Kobayashi, K. Fujita, Y. Kususe, Y. Matsushita, K. Tanaka, and H. Kageyama, *Inorg. Chem.*, 2015, **54**, 1501-1507.

18 D. Akahoshi, H. Horie, S. Sakai, and T. Saito, *Appl. Phys. Lett.*, 2013, **103**, 172407.

19 K. Jiang, J. J. Zhu, J. D. Wu, J. Sun, Z. G. Hu, and J. H. Chu, *ACS Appl. Mater. Inter.*, 2011, **3**, 4844-4852.

20 S. M. Xing, C. Shan, K. Jiang, J. J. Zhu, Y. W. Li, Z. G. Hu, and J. H. Chu, *J. Appl. Phys.*, 2015, **117**, 103107.

21 C. Shan, P. Chang, K. Shi, Y. W. Li, Z. G. Hu, and J. H. Chu, *RSC Advances*, 2014, **4**, 34987-34991.

22 K. Fujita, N. Wakasugi, S. Murai, Y. Zong, and K. Tanaka, *Appl. Phys. Lett.*, 2009, **94**, 062512.

23 L. S.-J. Peng, X. X. Xi, B. H. Moeckly, and S. P. Alpay, *Appl. Phys. Lett.*, 2003, **83**, 4592.

24 S. Kamba, V. Goian, M. Orlita, D. Nuzhnyy, J. H. Lee, D. G. Schlom, K. Z. Rushchanskii, M. Ležaić, T. Birol, C. J. Fennie, P. Gemeiner, B. Dkhil, V. Bovtun, M. Kempa, J. Hlinka, and J. Petzelt, *Phys. Rev. B*, 2012, **85**, 094435.

25 M. Allieta, M. Scavini, L. J. Spalek, V. Scagnoli, H. C. Walker, C. Panagopoulos, S. S. Saxena, T. Katsufuji, and C. Mazzoli, *Phys. Rev. B*, 2012, **85**, 184107.

26 R. Ranjan, H. S. Nabi, and R. Pentcheva, *J. Phys.: Condens. Matter*, 2007, **19**, 406217.

27 L. Sagarna, S. Populoh, A. Shkabko, J. Eilertsen, A. E. Maegli, R. Hauert, M. Schrade, L. Karvonen, and A. Weidenkaff, *J. Phys. Chem. C*, 2014, **118**, 7821-7831.

28 M. Rössle, C. N. Wang, P. Marsik, M. Y. Rizi, K. W. Kim, A. Dubroka, I. Marozau, C. W. Schneider, J. Humlíček, D. Baeriswyl, and C. Bernhard, *Phys. Rev. B*, 2013, **88**, 104110.

29 J. Yang, Y. Q. Gao, J. Wu, Z. M. Huang, X. J. Meng, M. R. Shen, J. L. Sun, and J. H. Chu, *J. Appl. Phys.*, 2010, **108**, 114102.

30 S. A. Lourenço, I. F. L. Dias, J. L. Duarte, E. Laureto, E. A. Meneses, J. R. Leite, and I. Mazzaro, *J. Appl. Phys.*, 2001, **89**, 6159.

Table of Contents (TOC). (a) The XRD patterns of ETO thin films measured at room temperature. Note that the (002) peaks from the annealed ETO films shift toward a higher angle side, indicating a relaxation of the out-of-plane lattice strain. (b) Schematic diagrams of the photo induced interband transitions. The dashed area indicates the change of the valence electric structures after the post-annealing process: the optical band gap E_1 increasing while the higher energy transition E_2 decreasing.